LANGMUIR

Phospholipid and Hydrocarbon Interactions with a Charged Electrode Interface

Zachary A. Levine,[†,‡,§] Nadica Ivošević DeNardis,[∥,§] and P. Thomas Vernier*[⊥]

[†]Department of Physics and [‡]Department of Chemistry and Biochemistry, University of California Santa Barbara, Santa Barbara, California 93106, United States

[∥]Division for Marine and Environmental Research, Ruđer Bošković Institute, Zagreb, Croatia

[⊥]Frank Reidy Research Center for Bioelectrics, Old Dominion University, Norfolk, Virginia 23508, United States

S *Supporting Information*

ABSTRACT: Using a combination of molecular dynamics simulations and experiments we examined the interactions of alkanes and phospholipids at charged interfaces in order to understand how interfacial charge densities affect the association of these two representative molecules with electrodes. Consistent with theory and experiment, these model systems reveal interfacial associations mediated through a combination of Coulombic and van der Waals forces. van der Waals forces, in particular, mediate rapid binding of decane to neutral electrodes. No decane binding was observed at high surface charge densities because of interfacial water polarization, which screens hydrophobic attractions. The positively charged choline moiety of the phospholipid palmitoyloleoylphosphatidylcholine (POPC) is primarily responsible for POPC attraction by a moderately negatively charged electrode. The hydrocarbon tails of POPC interact with the hydrophobic electrode interface similarly to decane. Previously reported electrochemical results confirm these findings by demonstrating bipolar displacement currents from PC vesicles adhering to moderately negatively charged interfaces, originating from the choline interactions observed in simulations. At more negatively charged interfaces, choline-to-surface binding was stronger. In both simulations and experiments the maximal interaction of anionic PS occurs with a positively charged interface, provided that the electrostatic forces outweigh local Lennard−Jones interactions. Direct comparisons between the binding affinities measured in experiments and those obtained in simulations reveal previously unobserved atomic interactions that facilitate lipid vesicle adhesion to charged interfaces. Moreover, the implementation of a charged interface in molecular dynamics simulations provides an alternative method for the generation of large electric fields across phospholipid bilayers, especially for systems with periodic boundary conditions, and may be useful for simulations of membrane electropermeabilization.
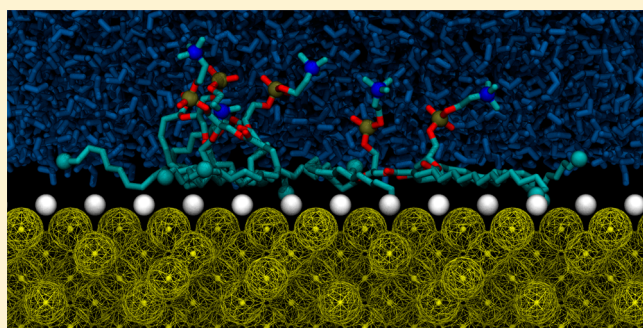
1. INTRODUCTION

Cell membranes partition the external aqueous environment from the cellular interior. Fundamental and systematic studies of the influence of electric potentials at the membrane interface are important for understanding how the barrier function of the membrane is implemented through the action of voltage-gated membrane proteins and the interactions of membrane constituents, primarily phospholipids and proteins.[1,2] Techniques employing the mercury electrode are widely used for membrane studies, due to mercury fluidity and easy control of surface properties by variation of applied potential. The phospholipids deposited on a mercury electrode surface, either by extruding the drop of mercury through a monolayer spread on a gas−solution interface or by unilamellar vesicle fusion, have been extensively studied.[2−6] The phospholipid monolayers undergo two pronounced phase transitions characterized by two capacitance peaks at potentials more negative than the point of zero charge of mercury interface as a result of competition between the heads and the tails for access to the

electrode interface[3] or due to the complicated reorientation from thin and thick monolayer to finally a porated bilayer.[4] Surface charge densities at the membrane interface play a crucial role for membrane fusion, uptake of therapeutic agents by targeted cells, and cell−ligand binding kinetics. Surface properties of membranes have been extensively investigated in studies of adhesion to charged and uncharged surfaces.[7−13] In particular, electrochemical amperometry utilizes a liquid mercury electrode to directly probe the surface charge densities of lipid vesicles and cells. Recently, we observed that phospholipid vesicle adhesion to a mercury electrode is highly dependent on the polar headgroup and on whether the lipid is zwitterionic or anionic.[12] Close contact of phospholipid polar head groups has been observed on gold electrode surfaces,[14,15] but very little is known about lipid adhesion to mercury

A

electrodes.[16] Reports have indicated that polar head groups in the outer surface of liposomes do not strongly alter the electrode charge density upon contact and that it is energetically unfavorable for lipid headgroups to orient themselves toward the mercury electrode, since it is hydrophobic.[17,18] These experimental indications of nanoscale interfacial interactions can be studied in atomistic detail in molecular dynamics (MD) simulations. We carried out unitedatom MD simulations of hydrated phospholipids near the surface of electrodes to investigate how charging of the interface affects lipid orientation and conformation and headgroup and hydrocarbon tail affinity to the interface. These results are compared to amperometric measurements of lipid vesicle adhesion to a dropping mercury electrode/ aqueous electrolyte interface. We place our results in the context of cellular regulation, fusion, and adhesion to nearby biological[19−21] or artificial[22] surfaces. These findings are also relevant for the development of new tools and techniques. For example, the integration of in situ renewable mercury microelectrodes into an atomic force microscope cantilever shows considerable promise for simultaneously measuring both interfacial forces and surface properties at biological interfaces.[23] The ability to probe atomistic lipid interactions with charged interfaces on nanometer length scales in simulations will enable optimization and construction of next-generation probes and sensors for analysis of biomembranes in physiological electric fields.

2. MATERIALS AND METHODS

2.1. Molecular Dynamics Conditions and Parameters. All simulations were performed using the GROMACS 4.5.5 software package[24] on the University of Southern California's High Performance Computing and Communications (HPCC) Linux cluster (http://hpcc.usc.edu/). Lipid headgroup topologies were derived from OPLS united-atom parameters;[25] lipid tails and decane were parametrized using the Berger united-atom force field.[26] Topologies were obtained from Peter Tieleman at the University of Calgary and can be obtained at http://moose.bio.ucalgary.ca. The simple point charge (SPC) water model was used as solvent.[27] Systems were coupled to a temperature bath at 310 K with a relaxation time of 0.1 ps using a weak coupling algorithm, while an NVT ensemble was maintained in order to maintain constant volume. An integration time step of 2 fs was used. Bond lengths were constrained using the LINCS algorithm for lipids and hydrocarbon[28] and the SETTLE algorithm for water.[29] Short-range electrostatic and Lennard−Jones interactions were cut off at 1.0 nm. Long-range electrostatics interactions were calculated with the PME algorithm using fast Fourier transforms and conductive boundary conditions. Reciprocal-space interactions were evaluated on a 0.12 nm grid with fourth-order B-spline interpolation. Periodic boundary conditions were employed to mitigate system size effects.

2.2. Molecular Dynamics Systems and Structures. Electrodes were constructed by placing 384 uncharged GROMOS05[30] silicon atoms in a diamond lattice configuration for the electrode bulk and 128 partially charged silicon atoms at the electrode surface. Silicon was chosen because it was well parametrized within the GROMOS force fields, while mercury (the material utilized in experiments) was not. Given the lack of electronic polarizability in simulations, we expect our simulations to be largely generalized to multiple electrode surfaces, including mercury electrodes. Charge magnitudes for surface atoms were set to 0, ±0.0625, ±0.2044, and ±0.4088 e in order to obtain surface charge densities of 0, ±2.77, ±9.06, and ±18.12 $\mu C/cm^2$, respectively. In this study we refer to these systems as uncharged, moderately charged, highly charged, and very highly charged. Simulation boxes were on the order of 6.8 nm × 6.8 nm × 14.9 nm and contain four electrode interfaces that enclose two regions of bulk

water (each about 5 nm in thickness). Surface charge density was negative on the top electrode (as seen in Figure 1), neutral on the
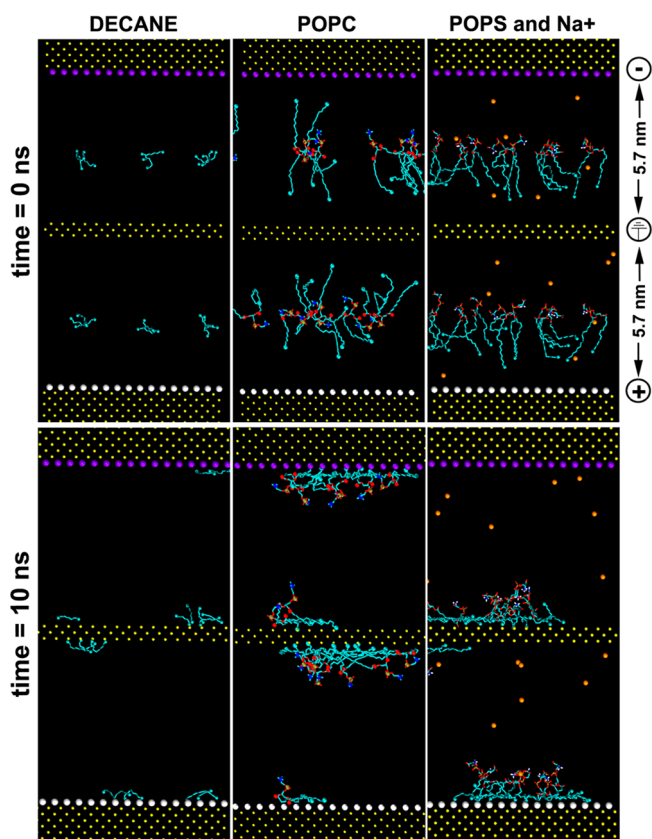

Figure 1. Representative snapshots of molecular dynamics simulation volumes containing decane, POPC, and POPS at the moderately charged interface, captured at the beginning and at the end of a simulation. White and purple spheres represent positively and negatively charged silicon atoms, respectively. Carbon atoms are cyan, oxygen atoms red, phosphorus atoms dark gold, and nitrogen atoms blue. Orange Na+ counterions can be seen in POPS systems.

central electrode, and positive on the bottom electrode, allowing us to observe the effects of both positive and negative polarities. Gauss's law then yields electric fields of magnitude 0, 3, 10, and 20 V/nm in vacuum. This translates to an effective electric field in water (relative dielectric permittivity = 80) of 0, 38, 125, and 250 MV/m, which is comparable to experimental electric field magnitudes.[31] Since we are interested in interactions with the electrode interface and not with the electrode bulk, we maintained the internal electrode geometry by freezing the positions of silicon in an ideal diamond configuration. Each system was then equilibrated for 10 ns to ensure that the charged interface was adequately hydrated and energy minimized.

Following equilibration, eight lipid or hydrocarbon molecules were randomly selected from a separate equilibrated bilayer structure containing 1-palmitoyl-2-oleoyl-sn-glycero-3-phosphatidylcholine (POPC), 1-palmitoyl-2-oleoyl-sn-glycero-3-phosphatidylserine (POPS), or decane. Molecules were then inserted along the midplane between electrodes to observe how zwitterionic, anionic, and uncharged molecules interact with a nearby charged interface (Figure 1). Systems containing POPS also contained an equal number of sodium counterions to maintain electrical neutrality. Triplicate 10 ns simulations were carried out for each system, with atoms assigned a random velocity from a Maxwell distribution at the beginning of the simulation.

2.3. Molecular Dynamics Analysis. Mass and local electric field profiles were generated from the GROMACS tools g_density and g_potential, with measurements taken every picosecond. Initial

profiles were averaged from the first nanosecond of simulations (i.e., immediately after the insertion of a lipid or hydrocarbon), and final profiles were averaged over the last nanosecond of simulation. Bound molecules were defined as any molecule with a terminal methyl carbon or carboxyl oxygen (POPS) within 0.3 nm of an interfacial silicon atom. Custom Perl scripts were used to measure atomic distances and molecular binding affinities to the interface. To determine the mean number of water molecules accumulated or displaced from the interface after lipid binding occurred, we compared the initial and final water densities at the interface and extrapolated the number of water molecules required to reproduce these changes in density.

2.4. Molecular Dynamics Images. Molecular graphics images were generated with Visual Molecular Dynamics (VMD).[32]

2.5. Hydrocarbon Droplet Dispersion. Aqueous dispersions of n-decane (180 mg/L) were prepared by shaking 50 μL of decane (99% GC, Aldrich) in 250 mL of 0.1 M NaF solution, containing 5 mM NaHCO$_3$, in order to maintain a pH of 8.4 for 1 h at 300 rpm. Polydispersity was characterized by Coulter counter measurements of freshly prepared decane dispersions. Size distributions of organic droplets were consistent in independent preparations and remained virtually unchanged over a period of 20 min, which was sufficient to run our electrochemical experiments.

2.6. Lipid Vesicle Suspensions. DOPC (1,2-dioleoyl-sn-glycero-3-phosphocholine) was purchased from Sigma Chemical Co. (St. Louis, MO, USA). Unilamellar DOPC vesicle suspensions were prepared according to the procedures outlined by Moscho et al.[33] Lipids were dissolved in chloroform (0.1 M), and 20 μL of the resulting solution was added into a 50 mL round-bottom flask containing 920 μL of chloroform and 150 μL of methanol. A 7 mL amount of phosphate-buffered saline (PBS) was then carefully added along the flask walls. Organic solvents were removed in a rotary evaporator under a pressure of 240−300 mmHg at 40−43 °C. After evaporation for 2 min an opalescent fluid was obtained, with a total volume of approximately 6.5 mL. The suspension was characterized with a Coulter counter using a 140 μm (diameter) sampling orifice tube, where particle size distribution was in the range 2−60 μm. PS (1,2-diacyl-sn-glycero-3-phospho-L-serine) from bovine brain (≥97%) was purchased from Sigma Chemical Co (St. Louis, MO, USA) and used as received. Multilamellar PS vesicles were prepared by dissolving 10 mg of lipid in 2 mL of chloroform. After rotary evaporation of the solvent the remaining lipid film was dried in vacuum for 1 h and dispersed by gentle hand shaking in 1 mL of PBS. The solution was left overnight at 4 °C to swell and stabilize. The suspension selected for electrochemical measurements was characterized by a Coulter counter to determine vesicle concentrations and size distributions using a 100 μm (diameter) sampling orifice tube. Size distributions were easily reproducible and stable throughout each experiment. Vesicle suspensions (2×10^8 particles/L) were predominantly sized from 3.2 to 16 μm.

2.7. Electrochemical Measurements. The dropping mercury electrode had a drop life of 2 s, a flow rate of 6 mg/s, and a maximum surface area of 4.57 mm^2. Potentials were measured against an Ag/AgCl (0.1 M NaCl) reference electrode, which was separated by a ceramic frit. Its potential was +2 mV versus a calomel electrode (1 M KCl). Electrochemical measurements were performed using a PAR 174A Polarographic Analyzer interfaced to a computer. Data was acquired with a DAQ card-AI-16-XE-50 (National Instruments) input device and processed with LabView 6.1. Current−time (I−t) curves over 25 mercury drop lifetimes were recorded at constant potentials (i.e., surface charge density) with a time resolution of 50 μs. Signal counts refer to the number of adhesion signals over 25 consecutive I−t curves (i.e., during 50 s). The majority of experiments were performed by aliquot addition of a stock solution in previously deaerated aqueous electrolyte solution under nitrogen purging for a few minutes at 25 °C. A series of experiments was carried out in air-saturated solutions.

2.8. Electrochemical Method. Chronoamperometry with a dropping mercury electrode enables detection of organic particles and living cells in aqueous samples as described previously.[9−13] Adhesion and spreading of micrometer-size particles at a charged mercury/water interface causes double-layer charge displacement to occur from the inner Helmholtz plane, where a transient flow of compensating current can be recorded as an adhesion signal. The key ingredient in such a measurement is the potentiostatic control of adhesion forces by changing the surface charge and interfacial tension at the electrode/aqueous electrolyte interface.[34,35] The adhesion force can then be fine tuned to study the interplay among the processes involved in deformable particle−electrode double-layer interactions. In particular, the signature of a single adhesion event at the mercury electrode is a transient current spike, which is consistent with the classical model of electrical double charge layers at the electrode/aqueous electrolyte interface. The double-layer charge displacement current of organic microdroplets at the mercury electrode reflects the dynamics of the spreading process and the wetting equilibria.[34,36] The Young−Dupré equation for the three-phase liquid system is applicable to the wetting equilibria of hydrocarbons at the electrified mercury/aqueous electrolyte interface.[34] The total Gibbs energy of interaction between a droplet and the aqueous mercury interface is $-\Delta G = A \cdot (\gamma_{12} - \gamma_{23} - \gamma_{13})$, where γ_{12}, γ_{13}, and γ_{23} are the interfacial energies at mercury/water, mercury/organic liquid, and water/organic liquid interfaces, respectively. The expression in parentheses is the spreading coefficient (S_{132}) at the three-phase boundary.[37] When $S_{132} > 0$, attachment and spreading are spontaneous processes; when $S_{132} < 0$, spreading is not spontaneous. The critical interfacial tension of adhesion $(\gamma_{12})_c$ defined by $S_{132} = 0$ will be $(\gamma_{12})_c = \gamma_{13} + \gamma_{23}$. In the case of nonpolar organic liquids, the measured critical interfacial tensions of adhesion at the positively and negatively charged interfaces are the same, showing good agreement with the calculated values[36] according to Young−Dupré and Good−Girifalco−Fowkes relationships.

3. RESULTS

3.1. Molecular Dynamics Simulations of Hydrocarbon and Lipid Interaction at Charged Interface.
In these molecular simulations we focused on the relative binding affinities of representative hydrocarbons and phospholipids at charged interfaces, which are (to first order) analogous to the charge-dependent adhesion affinities observed in experiments. Uncharged, moderately charged, and very highly charged interfaces (with surface charge densities equal to 0, ±2.77, and ±18.12 μC/cm^2, respectively) were simulated in the presence of either decane, POPC, or POPS, where three trials were carried out and averaged for each system. Decane and POPC were also simulated with the highly charged interface (±9.06 μC/cm^2) to better evaluate the transition from moderately charged to very highly charged interfaces.

3.1.1. Uncharged Interface. Decane binds quickly to the uncharged interface (within a few hundred picoseconds) in order to maximize its native hydrophobicity. Although weak van der Waals forces act between individual decane molecules, no large-scale hydrocarbon aggregation is observed in water, which suggests that binding to neutral surfaces is energetically favorable relative to clustering in bulk water. Because decane is electrically neutral, there is no preferential binding to the positively or negatively charged electrodes; all decane molecules are bound to the two surfaces within 4.5 ns of insertion into the system. Electrode-bound decane molecules assume a curved conformation. The terminal methyl groups are strongly bound (within 0.3 nm) to individual interfacial silicon atoms, while the middle of the decane molecule lies higher off of the interface (Figure 1). The decane center of mass is located just under a layer of interfacial water molecules (Table 1) on the hydrophobic electrode surface, thereby shielding the hydrocarbon from a number of bulk water interactions.

While bound to neutral electrodes, decane often "walks" or laterally hops across the surface from one silicon atom to another, alternating between its terminal methyl groups. When

Table 1. Water Orientation, Distance from Electrode, and Binding Time of All Molecules (expressed as average values) Are Shown at Various Surface Charge Densities[a]

electrode surface charge density (μC/cm^2)	mean interfacial water orientation (cos θ)	mean interfacial water distance to electrode (nm)	mean time to bind all molecules (ns)
uncharged (0.00)	positive int.: −0.35	positive int.: 0.05	decane: 4.6 ± 1.8
	negative int.: +0.23	negative int.: 0.18	POPC: 7.2 ± 1.8
			POPS: 5.5 ± 2.6
moderately charged (±2.77)	positive int.: +0.16	positive int.: 1.1	decane: 2.5 ± 0.5
	negative int.: +0.33	negative int.: 0.1	POPC: 4.2 ± 3.3
			POPS: 6.0 ± 0.5
highly charged (±9.06)	positive int.: +0.46	positive int.: 0.1	decane: 2.5 ± 0.5
	negative int.: +0.53	negative int.: 1.1	POPC: 5.0 ± 2.6
very highly charged (±18.12)	positive int.: +0.62	positive int.: 1.1	decane: >10
	negative int.: +0.73	negative int.: 2.1	POPC: 4.8 ± 0.8
			POPS: 0.5 ± 0.1

[a]Interfacial water measurements corresponded to the adjacent water density peaks found next to the interface in Figure 5.
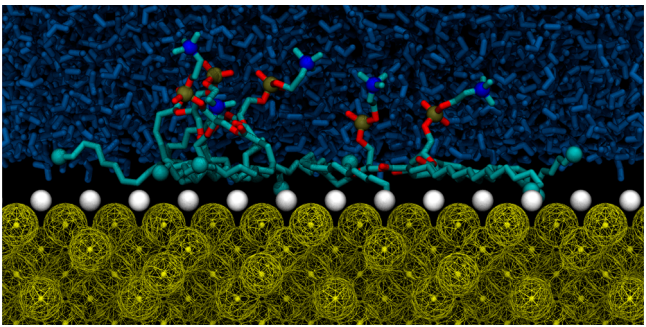

Figure 2. Five POPC molecules bound to an uncharged interface. Lipid tails stretch out along the electrode under the water hydration layer to maintain tail hydrophobicity and ensure terminal methyl binding, while the glycerol backbone is free to bind directly to the interface.

carbon atoms and the glycerol groups (Figures 2 and 3). This behavior reduces the hydration of lipid tails, similar to what was
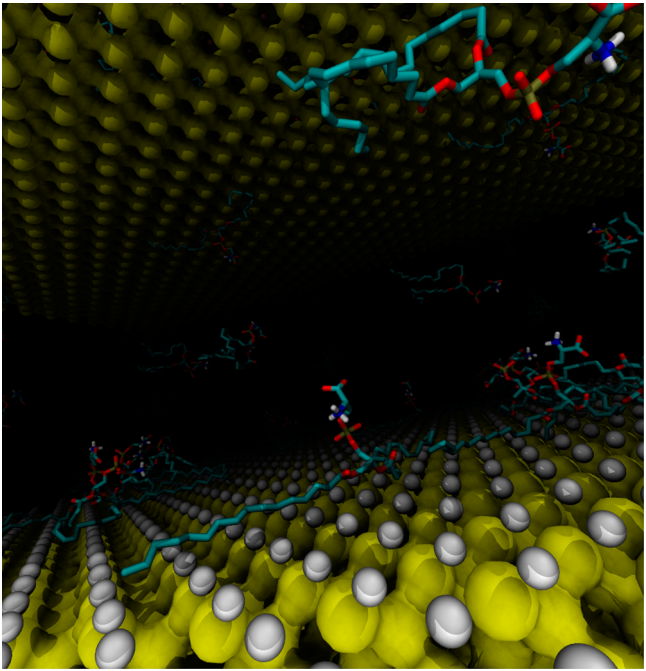

Figure 3. PS binds equally to all neutral surfaces, both individually and in clumped aggregates. Lipid conformations observed here, however, are similar to those exhibited by PC upon binding to moderately charged interfaces.

a bound decane molecule approaches another bound decane (within 0.2 nm) they do not cross over one another. The energy required to lift a decane into water and over its neighbor is greater than that required for lateral diffusion (at room temperature) in another direction. We also observe a slight preference for water hydrogens to be orientated toward neutral interfaces, while water oxygens tend to be directed slightly away from the interface.

More precisely, if we define for each water molecule a vector pointing from the water oxygen atom to the center of geometry between the water hydrogen atoms we observe average water orientations of only about 17° toward the plane of each interface, where 0° represents no directional affinity toward any surface. (This can also be seen by measuring net water dipole moments at each surface relative to the z direction (Table 1), where the sign of each value corresponds to either the top electrode (when the dipole moment is positive) or the bottom electrode (when the dipole moment is negative). This same convention is used in subsequent figures, where the top of the simulation box is considered the positive z direction, while the bottom of the simulation box is considered the negative z direction.)

For lipids at uncharged interfaces, POPC binds (on average) more slowly than decane (7.2 ns for POPC, 4.6 ns for decane). Binding to the interface occurs predominantly through Lennard−Jones interactions between individual silicon atoms and both the sn-1 and the sn-2 terminal carbon atoms of POPC (Figures 1 and 2) and is likely stabilized by low water entropy at the nonpolar surface. There is also a slight attraction between acyl oxygen atoms on the glycerol lipid backbone and the neutral interface, which encourages lipid tails to lie parallel to the surface in order to make contact with both the terminal

observed for decane. Lipid head groups prefer to remain hydrated in bulk above the silicon surface, generally in perpendicular orientations relative to the surface, about a nanometer from individual silicon atoms (Figure 3). Similar to decane, bound lipid tails rarely cross one another after binding to the surface occurs (unless a lipid tail initially lands on top of an already bound tail). In both PC and PS systems, however, we observe the formation of multiple small lipid aggregates in bulk water. These aggregates (with their lipid tails directed inward) eventually bind to the two uncharged interfaces. PC and PS aggregates can bind to the interface while maintaining their spherical, bulk aggregate morphology, thus minimizing interactions between hydrophobic lipid tails and water. PS systems exhibit binding characteristics similar to PC systems
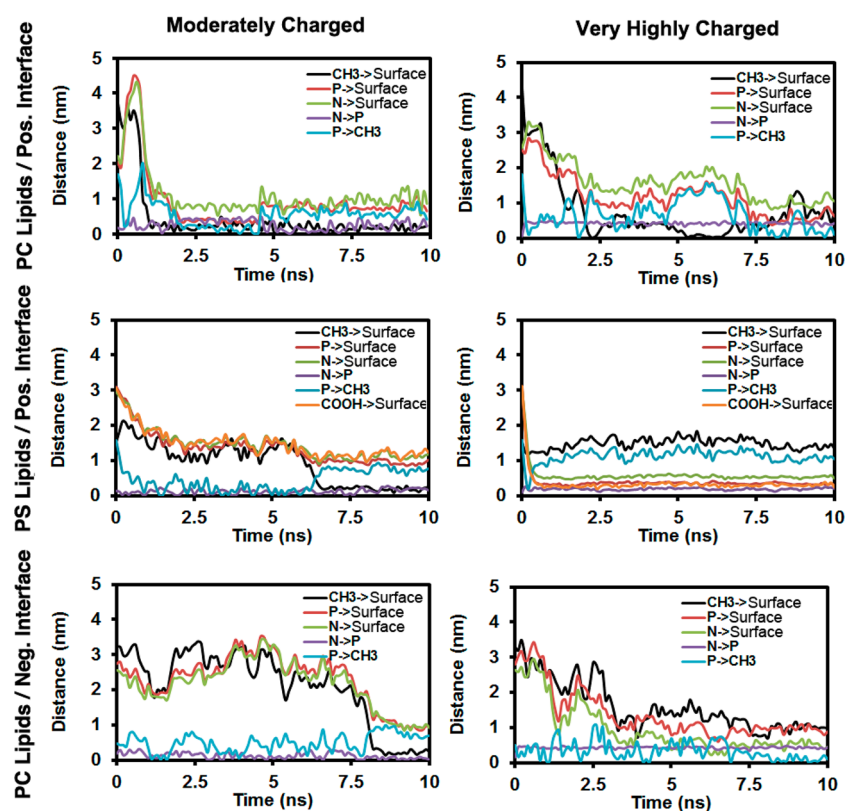
Figure 4. Distances between particular chemical groups as a function of simulation time from the moderately charged interfaces (left) and very highly charged interfaces (right).

near the neutral interface. The PS head groups electrically repel one another, which decreases bulk aggregation and speeds up binding to the interface ($t_{binding}$ = 5.5 ns) compared to PC systems.

3.1.2. Moderately Charged Interface. In moderately charged systems, decane binds quickly to the interface. All eight molecules are bound within 2.5 ns. Decane molecules in the bulk water do not aggregate, but they clump together after binding to the interface. The mean dipole angle of water near the electrode interface (Table 1) orients toward the electric field on both interfaces. The average water orientation—cos θ, where θ is measured relative to the z direction)—near the negatively charged interface increases slightly from 0.23 (in the uncharged system) to 0.33, while water near the positive interface rotates from cos θ = −0.35 (in the uncharged system) to cos θ = 0.16, both in the direction of the resulting electric field.

Both decane and POPC, but not POPS, bind more quickly to the moderately charged interface than to the uncharged interface (Table 1). While this might seem counterintuitive, POPS aggregates in larger quantities near moderately charged interfaces compared to POPC, where the time required for the construction of PS aggregates increases the total time it takes for all PS to eventually bind to the interface. For PC lipids, aggregation occurs more quickly since there is no electrostatic repulsion between zwitterionic head groups; thus, PC aggregation and subsequent binding is quicker in these systems than PS. Additionally, interfacial water at the positive electrode (to which the anionic POPS is attracted) must first rotate in a concerted manner away from the surface, which complicates the interfacial electrostatic landscape. In PC systems, many of the lipids are also attached to the opposite electrode where

water rotation does not occur; therefore, binding occurs more quickly. Lipid aggregation in bulk water also delayed binding in some trials (Figure 4). On average, decane and POPC do not show a polarity preference, but POPS significantly prefers binding to the positively charged electrode (Figures 1 and 5), as one would expect. Furthermore, sodium counterions in POPS simulations tend to associate with the negative electrode. Representative binding curves for the uncharged system (Figure 6, left) and the moderately charged system (Figure 6, right) are also displayed. While individually bound POPS molecules migrate quickly to the interface due to strong electrostatic attractions (Figure 6F), POPS aggregates must disassemble once they arrive at the positively charged interface, often retaining some of their clumped morphology while attempting to minimize surface interactions with water. Compared to the analogous uncharged system containing POPS (Figure 6C), where individual lipids bound more slowly to the neutral interface, total binding of all lipid molecules to moderately charged surfaces occurred on similar time scales.

In systems containing POPC, negatively charged phosphates are initially attracted to the positively charged electrode. However, binding occurs only after the lipid rotates and attaches its terminal methyl group to a charged interface atom (Figure 4). This is different from binding on the negatively charged electrode, where the POPC phosphate is somewhat repelled by the interface. After the lipid tail binds, however, POPC head groups remain at a constant distance from the negatively charged interface, which is similar in magnitude to the separation maintained from the positively charged interface. PS carboxyl groups, however, do not strongly bind to the positively charged interface, primarily due to the lack of
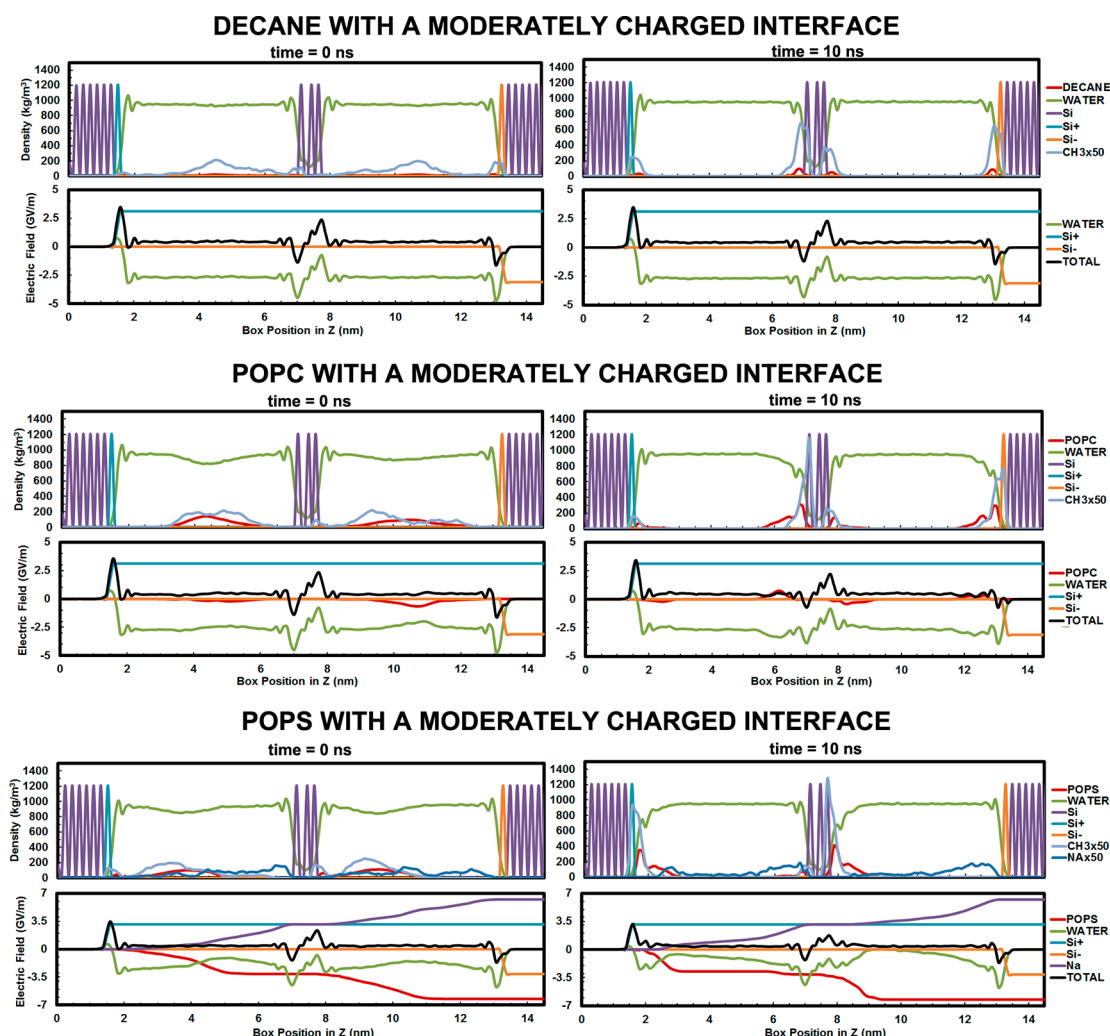
Figure 5. Density and local electric field profiles for moderately charged interface systems as a function of box length, extracted from representative molecular dynamics simulations of decane, POPC, and POPS. Left panels correspond to the beginning of the simulation, and right panels correspond to the end of the simulation.

401 hydrating water molecules, despite the electrostatic attraction to
402 the electrode.

403   *3.1.3. Highly Charged Interface.* Behavior observed in
404 highly charged interface systems is intermediate between that
405 observed at the moderately charged and very highly charged
406 interfaces. Initially decane forms a number of aggregates in the
407 water bulk; however, complete binding to the interface is still
408 observed within a few nanoseconds, as it is for the weakly
409 charged and neutral interfaces. Binding times of decane to
410 highly negative or highly positive interfaces are similar to those
411 for the moderately charged interface (since decane does not
412 interact electrically with the electrodes); however, some
413 features have changed. Regarding water, the orientation of
414 bound water near the electrode surface increases steadily to cos
415 θ = 0.46 on the positive surface and cos θ = 0.53 on the
416 negative surface. This is important because while we may not
417 detect large differences in the binding behavior of lipids, we can
418 see steady increases in water polarization near the electrode as
419 the charge density is increased. In the asymptotic case, we
420 might expect that when interfacial water is highly polarized at
421 the electrode, changes to lipid binding behavior occur. While
422 hydrating water orientation is affected by changes in surface
423 charge density, the location of those water molecules relative to

424 the electrode is unchanged across all charge densities tested in
425 this study (Table 1). Bound decane molecules begin to
426 aggregate on highly charged electrode long after they are fixed
427 to the surface. This process is driven by surface diffusion and is
428 stabilized through Lennard–Jones potentials. These bound
429 aggregates, however, were not observed on less charged
430 interfaces. The morphology of bound decane aggregates on
431 the highly charged surface resembles a hemisphere, which
432 maximizes hydrophobicity in its interior, similar to the
433 morphology of bound decane molecules on uncharged surfaces.
434 Multiple bound decane molecules were able to cross over one
435 another on the highly charged interfaces, in contrast to their
436 behavior on uncharged and moderately charged interfaces.

437   POPC aggregates (consisting of 5−6 lipids) form in the
438 highly charged interface systems, both in the bulk solution and
439 on the electrode after binding occurs. Electrostatic attraction
440 between positively charged POPC choline and the negatively
441 charged interface also begins to increase, to the extent that a
442 number of PC lipids are bound to the negative interface by
443 both their head and tail regions (Figure S1, Supporting
444 Information). Additionally, POPC aggregates sometimes
445 anchor themselves to the interface by only a single choline
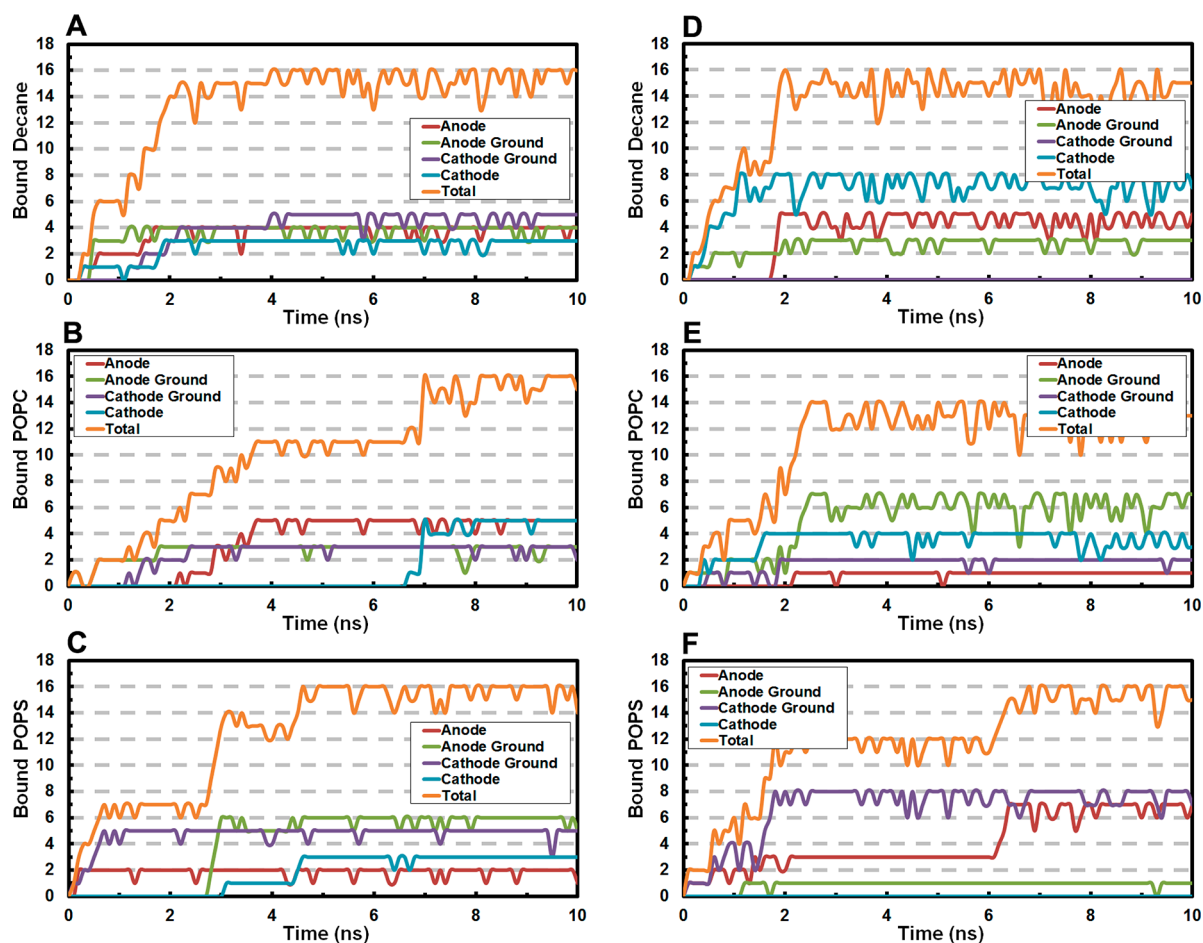446 group or a single methyl group, following which the rest of the

Figure 6. Numbers of molecules bound to the uncharged interface (A–C) and to the moderately charged interface (D–F) as a function of time. Values are taken from representative molecular simulations, which yield slightly different values from the numbers listed in Table 1, which are the average of multiple simulations. Here, "anode" refers to the positively charged interface, while "cathode" refers to the negatively charged interface.

aggregate is slowly pulled toward the interface. Once a POPC aggregate is bound to the electrode, its final shape (hemispheric radius) appears to be determined by the distance between the glycerol acyl oxygen atoms and the electrode. On the negatively charged interface, the electron-dense acyl oxygen is repelled, but binding mediated by POPC terminal methyl groups stabilizes spherical or hemispherical aggregates on the surface. On the highly positively charged interface the acyl oxygen atoms are bound, and this results in flatter aggregate morphologies on the surface, although the shapes and sizes of these clusters fluctuate. Overall, electrostatic forces appear to be balanced by van der Waals forces on the highly charged interfaces, since no one force dominates lipid binding in these systems.

3.1.4. Very Highly Charged Interface. At the highest charge densities examined we see new behaviors emerge, dominated by electrostatic forces. Although decane continues to aggregate in bulk water, these aggregates remain distant from the electrode rather than binding to the interface to minimize water contact. Hyperpolarized water molecules near the electrode (Table 1) appear to reduce decane binding by blockading entry to the hydrophobic interior; however, there are brief interactions between decane and the interface that can last for several nanoseconds (Figure 7). Decane aggregates consist of nearly parallel strands of adjacent hydrocarbons, in amorphous clumps with hydrophobic interiors rather than the
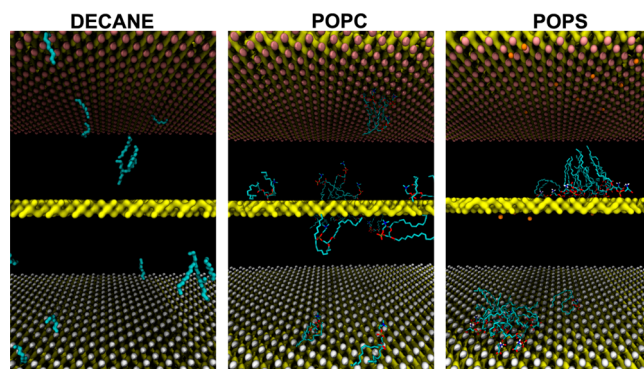

Figure 7. Representative snapshot from a molecular simulation showing the behavior of decane (left), POPC (middle), and POPS (right) near very highly charged electrodes. Orange Na^+ counterions can also be seen in PS systems.

hemispherical structures observed with the less charged interfaces. We did not observe convergent binding profiles for decane on very highly charged interfaces over the time scale of our simulations, indicating that hydrocarbon binding is severely reduced on the very highly charged interface.

Phospholipids, however, bind very quickly to the very highly charged interface, often in new conformations that are not observed on more weakly charged interfaces. After binding, the net headgroup dipole moment is strongly aligned in the

direction of the electric field (Figure 4). Although there is transient contact between lipid tails and the electrode interface, these relatively weak interactions (in the presence of such large charge magnitudes) are unstable. A number of POPC molecules also bind to the very highly positively charged interface through a combination of hydrophobic (tail) interactions and electrostatic (acyl oxygen) interactions, similar to what is observed at the highly charged interface. POPS binds even more quickly to the very highly positively charged interface (in less than a nanosecond), driven by the electrostatic attraction of the carboxyl oxygens in the serine residue of the headgroup. Lipid tails remain extended in bulk solution (Figure 7). Similarly, sodium counterions become immediately bound to very highly negatively charged interfaces on a time scale similar to that for POPS binding to positive interfaces. Bound POPS also heavily aggregates on very highly positively charged interfaces.

3.2. Electrochemical Adhesion-Based Detection of Hydrocarbon Droplets and Lipid Vesicles at Charged Interfaces.

Adhesion behaviors of decane droplets and PC and PS vesicles across a wide range of surface charge densities at the mercury/aqueous electrolyte were examined (Figure 8). Decane, which serves as a simple model molecule, is fluid at room temperature and is the shortest *n*-alkane which spontaneously adheres to and subsequently spreads across mercury interfaces.[36] Fluoride electrolyte was selected to avoid interference from the specific adsorption of ions on adhesion of decane droplets at the interface. The surface charge density range for decane adhesion is between −4.2 and 3.7 μC/cm^2, which corresponds to the most negative and to the most positive surface charge density where at least one adhesion signal is recorded per 10 consecutive $I-t$ curves. Beyond this range, adhesion of decane was not detected and droplets behaved as inert particles due to the stronger interaction of mercury with water and ions than the interaction with the decane. (i.e., $S_{132} < 0$). Whether adhesion and spreading will be favorable or not depends on the sign of the spreading coefficient. For $S_{132} > 0$, spreading is a spontaneous process because the interaction of droplet with water is stronger than cohesive forces between droplets. Decane, a nonpolar organic liquid, cannot be expected to interact with a water or mercury interface except by van der Waals or London dispersion forces which contribute to interfacial energy at the liquid/liquid interface. The importance of dispersion forces in hydrocarbon interaction with the mercury and water interface was previously demonstrated by the equal critical interfacial tension of wetting at positively and negatively charged interfaces.[36] The magnitude of droplet signal counts also changes considerably as the surface charge density of the electrode changes. Signal counts can be considered as a measure of adhesion affinity of soft particles which depends on the surface charge densities at the interfaces. Signal counts were determined by immersing the mercury electrode in an aerated dispersion and then in the deaerated dispersion. When measurements were performed with aerated dispersions, adhesion signals of decane droplets were detected as a transient enhancement of oxygen reduction.[38] Signal counts of decane droplets reach a maximum near zero surface charge density, where the interfacial tension of the mercury/aqueous electrolyte interface is close to its maximum value, at which point hydrophobic interactions are expected to dominate droplet adhesion. This sensitive mode of measurement can be used to examine adhesion affinity at a neutral interface (dotted line, Figure 8). When measurements were performed with
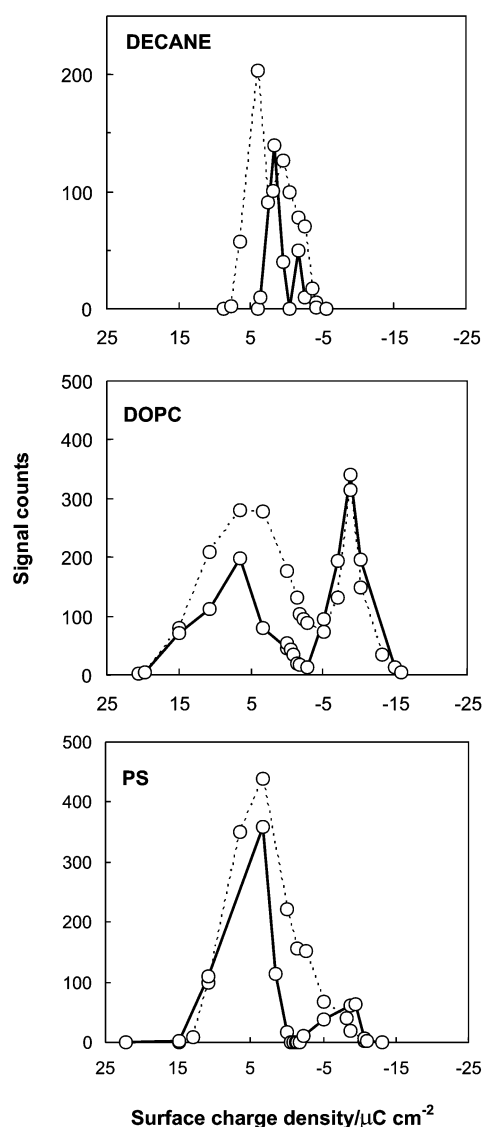

Figure 8. Dependence of adhesion signal counts on surface charge densities at the mercury/aqueous electrolyte interface as determined from chronoamperometric measurements. Thick lines and dotted lines correspond to measurements performed in deaerated and aerated solutions, respectively.

deaerated dispersions (in the absence of Faradaic oxygen reduction), signal counts for decane droplets rapidly decreased to zero at the uncharged interface, indicating that there is no electrode double layer to be displaced.

In contrast to the narrow adhesion range of decane, zwitterionic DOPC vesicles at mercury/PBS interfaces adhere across a wide range of surface charge densities (from −15.8 to 20.5 μC/cm^2). Adhesion signal counts for unilamellar DOPC vesicles were higher at negatively charged interfaces compared to positively charged ones. Minimum signal count charge for DOPC vesicles was shifted negatively by 2.7 μC/cm^2 from the point of zero charge of the mercury interface, which was detected also in systems of DMPC vesicles and egg-PC vesicles. This shift from the point of zero charge has been discussed in terms of polar headgroup orientation in the monolayer specifically in terms of electrostatic interaction of positively charged choline groups at the negatively charged mercury interface.[12] Such an effect of negative shift with respect to the

point of zero charge was observed for adsorption of phospholipid molecules onto the gold electrode as shown from the charge−potential curve.[39] Those investigators reported that applied potential to the electrode affects the properties of the bilayer, causing a transition from a compressible to a noncompressible state of bilayer. While in the desorbed state, the bilayer remains supported on gold, separated from the metal by a 1 nm aqueous layer. It was found that the potential shift depends linearly on the concentration of phosholipid molecules in the bilayer while the asymmetry of the surface potentials of the two leaflets of the bilayer[4] (one facing electrode and another one facing bulk solution) has to be small.

Adhesion of PS vesicles at the mercury/PBS interface was detected from −11.0 to 14.9 $\mu C/cm^2$ in deaerated suspension. As expected, signal counts of the negatively charged PS vesicles were higher at positively charged interfaces. By amperometric scanning of the applied potential at the mercury electrode to a point of no net current flow, the charge density of phospholipid vesicles which compensates electrode charge density could be determined. Adhesion signal counts of PS vesicles decreased to zero in the confined range from −0.55 to −1.50 $\mu C/cm^2$, where electrostatic interactions were identified. Adsorption of sodium and potassium ions from the PBS electrolyte solution (0.15 M) could play a significant role. Partial charge compensation might also result from the orientation of the most exposed positively charged ammonium groups of PS close to the charged interface. The charge compensation approach was previously used to determine the surface charge of cells, where the only hypothesis is the validity of the classical electrical double-layer model in terms of charge distribution at the electrode/solution interface.[10] Guidelli and co-workers reported that the charge density of a phospholipid monolayer deposited on a mercury electrode[40] passes from slight negative to slight positive values as pH is varied from 7.5 to 3. To determine the contribution to the membrane charge from PS, one must know the intrinsic protonation constants of the ionizable groups on PS. Intrinsic protonation constants of negatively charged groups in self-organized films of PS are significantly lower than the value determined with reference to the bulk pH, because the surface pH is less than the bulk pH. Conformation of the polar headgroup of PS and the intrinsic protonation constants of the ionizable groups are strongly sensitive to experimental conditions.

4. DISCUSSION

In this study we show how molecular simulations can enhance our understanding of the interactions of phospholipids with charged interfaces in real systems like the dropping mercury electrode. The behavior of the simple molecule *n*-decane provides a reference point for our approach and validates the theoretical force fields used in our molecular models against known experimental outcomes. In simulations, decane molecules are adsorbed most quickly onto neutral surfaces due to the dominance of hydrophobic interactions in the absence of strong electrostatic forces. At the point of zero charge, the macroscopic droplet of hydrocarbon forms a plano-convex lens occupying the largest contact area at the interface, due to the fact that interfacial tension is at a maximum, and van der Waals interactions prevail in adhesion of droplets to the mercury interface.[35] The maximum binding affinities of decane molecules in simulations and the maximum signal counts of decane droplets in experiments were both observed at

moderately charged interfaces. No decane binding occurred at the very highly charged interface, due to the dominance of interfacial water interactions with the electrode, as found both in simulation and in experiment. While a large number of studies have investigated the orientation and hydrogen-bonding strength of interfacial water molecules on fixed hydrophobic and hydrophilic interfaces,[41−43] water dynamics on highly charged interfaces (at voltages required for membrane permeabilization) are hotly contested. Due to the excellent agreement between the experimentally determined critical interface wetting tension of decane with calculated values using the Young−Dupré equation for three-phase liquid systems, it follows that macroscopic properties of decane govern the interfacial interaction of microscopic droplets at the charged electrode/aqueous interface.[36] Our simulation results are also consistent with interactions of phospholipid polar head groups with neutral mercury and gold electrodes, which have been reported previously through fluorescence quenching,[44] STM studies,[15] and amperometric detection of the bidirectional signal of DOPC vesicles.[12,16] Additionally, insight into phospholipid polar headgroup orientation and behavior of water molecules under the influence of electric field is of relevance for electropore formation in the lipid bilayer.[45]

The utilization of explicit electrodes for the application of external electric fields in simulations is significantly more robust than alternative methods that are found in most major MD integrators. Traditionally, electric fields are applied to simulations by adding a global force vector (with magnitude qE, where q is the charge associated with a given atom and E is the magnitude of the external electric field)[46] to each and every atom in the system. Unfortunately, this complicates the periodic boundary conditions present at each of the box ends, which are supposed to be held at similar physical conditions. If an external electric field is applied, the potentials on opposite ends of the box must be held at different (often high) values. Despite these complications, this process can be implemented with the understanding that the field, and not the potential, is the physical property that must be held constant at both ends. Indeed, as long as the potential difference or slope on one end of the box matches the slope on the opposite end, problems can be avoided. However, the introduction of global external electric fields tend to polarize water molecules at the ends of the box; therefore PME (as described in the Materials and Methods section), which tabulates long-range electrostatic potentials in Fourier space, adds a compensating surface charge density to offset the resulting net system dipole moment, thereby allowing PME to function correctly on an electrically neutralized simulation box. This methodology produces unexpected results, however, since the compensating surface charge (or dipolar) term in PME is dependent on the presence of aqueous interfaces, which may affect proper calculation of the MD Virial. The utilization of explicit charged electrodes, on the other hand, produces a truly neutral simulation box, since the resulting electric field stems from the presence of an equal number of positive and negative charges. Therefore, these systems are optimal for use in simulations where the inclusion of external electric fields is necessary.[47]

These results in small simulation boxes also provide insight into the behavior of phospholipids in confined volumes, where studies have shown that proteins change their conformations in the presence of solid-state surfaces like graphene.[48] While protein structures significantly differ from phospholipid structures, similar trends can be observed in their behavior

near solid surfaces: (1) interactions of hydrophobic moieties (e.g., lipid tails and aromatic protein residues) with synthetic surfaces, (2) conformational changes in bound molecules versus those in bulk solution, and (3) preferential electrostatic binding of charged chemical groups (e.g., lipid head groups or acidic or basic amino acid residues) to oppositely charged interfaces. To extend these initial, qualitative observations in future studies, more complex simulation techniques such as replica-exchange MD[49] may be required in order to adequately quantify the energy landscapes that are present at synthetic and biological interfaces. In addition, we will want to understand how the behavior at organic ("fouled") surfaces (e.g., self-assembled monolayers) differs from what we observe at simple solid-state interfaces like the ones studied here, since synthetic surfaces usually do not remain pristine in hostile aqueous environments. So-called "soft" systems are likely to yield dynamics that are different from "hard" interfacial systems, since fluctuating organic interfaces are often much better at conforming to nearby molecular geometries, thereby facilitating different binding kinetics.[50]

In simulations with moderately charged interfaces the strong attraction of the positively charged choline groups of POPC to the negatively charged surface draws phospholipids and phospholipid aggregates toward the interface. Under these conditions the electrode interface is sufficiently hydrophobic to attract the lipid tails through van der Waals forces. This balancing of electrostatic and van der Waals forces is observed for the first time in atomistic detail in these simulations, allowing us to decompose the macroscopic picture of lipid vesicle adhesion at charged interfaces into a combination of simple physical interactions. Simulations also reveal the unique lipid conformations that maximize the dehydration of the hydrocarbon tails and at the same time allow the polar heads groups to be hydrated in close proximity to the electrode. This behavior displaces a certain number of water molecules from the interface, and we can hypothesize that in a system containing electrolyte this will be associated also with the displacement of surface charges, producing subsequent displacement currents that can be measured experimentally.

At high and very highly negatively charged interfaces, choline headgroup binding is strongest, even compared to the moderately charged interface, where van der Waals forces might be expected to reinforce headgroup binding. Manifestation of electrostatic interactions for zwitterionic DOPC vesicles in close molecular contact with the charged mercury electrode is shown in the wide range of surface charge density based on the facts that (i) critical interfacial tensions of vesicle adhesion at the positively and negatively charged electrode are not equal, (ii) at the point of zero charge, signal counts does not drop to minimum, (iii) the minimum of adhesion signal counts is shifted negatively from the point of zero charge, and (iv) the appearance of a bidirectional signal of DOPC vesicles in the narrow surface charge density range.[12] Simulations of anionic PS molecules at positively charged interfaces also show distinct binding affinities where sodium ions are under some conditions transiently associated with lipid headgroups.[12,51] Surface charge density at the membrane depends on the aqueous electrolyte composition and pH. For 0.1 M sodium chloride at pH 7 a competition in the adsorption between the H^+ and the Na^+ ions takes place. The increased sodium ion concentration is associated with a decrease in the negative charge, consistent with the adsorption of Na^+. However, both simulations and experiments agree that maximal PS adhesion

occurs on the positively charged interface, where electrostatic forces outweigh Lennard−Jones interactions. Further, PS binding at an uncharged interface (Figures 1 and 7) could support the idea of charge compensation of PS vesicles in the vicinity of the point of zero charge (Figure 8). (i) PS molecule showed affinity to interact at the neutral electrode in the cathode compartment binding with tails, while the distance of the positively charged ammonium group varied between 0.6 and 1.4 nm (Figure 1, moderately charged interface). Measured double-layer charge displacement takes place at a distance of less than 1 nm; therefore, it might be possible to probe the charge which corresponds to the ammonium group on the PS. (ii) Sodium ions become entrapped in the headgroup region of PS, affecting the overall vesicle charge. (iii) Reversed orientation of PS binding with polar head groups at neutral electrode in the cathode compartment is shown at the very highly charged interface, Figure 7.

Therefore, simulations provide detailed insight into the interfacial behavior of polar head groups and hydrophobic tails of phospholipids in response to different surface charge densities, which is important for understanding the electro-chemical findings. We note the discrepancy in binding affinities between experiment and simulation of lipids at very high surface charge densities, which could be ascribed to the specific adsorption of anions at the positively charged interface,[36] taking into account the stochastic nature of that process. Also, although we do not expect that there will be large differences in general interfacial behavior between saturated and unsaturated lipid tails (POPC was used in simulations, DOPC in experiments), it is possible that there could be subtle differences between the simulation and the experimental results beyond those mentioned in this study. Since the critical interfacial tensions of adhesion are sensitive to the composition of hydrocarbon chains and specific polar groups of lipid vesicles, a less favorable interaction between POPC and mercury in comparison with DOPC might be expected, which would have an effect on the molecular orientation and packing in the monolayer. To compensate for these one could also include explicit displacement currents in simulations to better match the experimental conditions; lipid adhesion, however, is expected to correlate with the displacement currents measured near interfaces. If double charge layers are explicitly included in simulations then the displacement of ions at the surface due to hydrocarbon or lipid binding should produce currents similar to those observed in electrochemical experiments. Our results are consistent with the behavior of related systems such as adsorption of ionic surfactants on gold electrodes, specifically potential-controlled transformation of hemimicellar aggregates into a condensed monolayer at the electrode.[52] Finally, these results can also be placed in the context of the electropermeabilization of biomembranes.[13] The resting potential across a living cell membrane produces an electric field magnitude of roughly 25 MV/m, corresponding to a surface charge density of about 2 $\mu C/cm^2$ in our systems. Permeabilizing transmembrane voltages can be as low as 400 mV (~100 MV/m, or 8 $\mu C/cm^2$); therefore, the field magnitudes used in this study can be used to permeabilize membranes, where subsequent studies could reveal how ejected membrane lipids interact with nearby electrode surfaces. Systems containing explicitly charged electrodes, like those used in this study, may be useful for simulating these processes, in addition to a wide variety of other electropermeabilization phenomena.[47]

5. CONCLUSION

This study demonstrates how interface charge modulates the interfacial behavior of lipids. Molecular dynamics simulations reveal the nanosecond kinetics of phospholipid and hydrocarbon interactions with charged interfaces. Binding affinities in simulations are in agreement with independent electrochemical adhesion behavior, providing evidence at the molecular level important for understanding the fundamental mechanism of lipid vesicle adhesion at the charged interface. Unique lipid conformations and orientations are also observed, which affect the local electrostatic environment in the vicinity of the surface. The use of explicit electrodes in simulations also allows for self-consistent external electric fields to be introduced into simulations, which allows for proper particle mesh Ewald summation. This is a considerable improvement to existing electric field implementations, which rely on global perturbations to the Hamiltonian, and are thus incompatible with proper Ewald summation. Insight from simulations can be used to better understand the complex macromolecular structures that form on the charged interfaces and can be used to evaluate how both pristine and fouled electrodes affect a wide variety of biological systems both near and far from the electrified interface. The molecule−surface interaction energy could be explored more rigorously in future studies by applying quantum mechanical calculations of the electron density of atoms.

■ ASSOCIATED CONTENT

Ⓢ Supporting Information

The Supporting Information is available free of charge on the ACS Publications website at DOI: 10.1021/acs.langmuir.5b04090.

Snapshots from a molecular simulation showing the behavior of PC molecules near highly charged electrode interfaces (PDF)

■ AUTHOR INFORMATION

Corresponding Author

*E-mail: pvernier@odu.edu.

Author Contributions

§Z.A.L. and N.I.D. contributed equally to this work.

Notes

The authors declare no competing financial interest.

■ ACKNOWLEDGMENTS

■ REFERENCES

(1) Jones, S. W. Overview of Voltage-Dependent Calcium Channels. *J. Bioenerg. Biomembr.* **1998**, *30*, 299−312.

(2) Guidelli, R.; Aloisi, G.; Becucci, L.; Dolfi, A.; Monicelli, R.; Buoninegni, F. T. Bioelectrochemistry at Metal | Water Interfaces. *J. Electroanal. Chem.* **2001**, *504*, 1−28.

(3) Nelson, A.; Leermakers, F. A. M. Substrate-Induced Structural Changes in Electrode-Adsorbed Lipid Layers: Experimental Evidence from the Behavior of Phospholipid Layers on the Mercury-Water Interface. *J. Electroanal. Chem. Interfacial Electrochem.* **1990**, *278*, 73−83.

(4) Bizzotto, D.; Nelson, A. Continuing Electrochemical Studies of Phospholipid Monolayers of Dioleoyl Phosphatidylcholine at the Mercury-Electrolyte Interface. *Langmuir* **1998**, *14*, 6269−6273.

(5) Stauffer, V.; Stoodley, R.; Agak, J. O.; Bizzotto, D. Adsorption of DOPC onto Hg from the G|S Interface and from a Liposomal Suspension. *J. Electroanal. Chem.* **2001**, *516*, 73−82.

(6) Nelson, A. Electrochemistry of Mercury Supported Phospholipid Monolayers and Bilayers. *Curr. Opin. Colloid Interface Sci.* **2010**, *15*, 455−466.

(7) Godin, C.; Caprani, A. Interactions of Erythrocytes with an Artificial Wall: Influence of the Electrical Surface Charge. *Eur. Biophys. J.* **1996**, *25*, 25−30.

(8) Godin, C.; Caprani, A. Effect of Blood Storage on Erythrocyte/Wall Interactions: Implications for Surface Charge and Rigidity. *Eur. Biophys. J.* **1997**, *26*, 175−82.

(9) Svetličić, V.; Ivošević, N.; Kovač, S.; Žutić, V. Charge Displacement by Adhesion and Spreading of a Cell: Amperometric Signals of Living Cells. *Langmuir* **2000**, *16*, 8217−8220.

(10) Svetličić, V.; Hozić, A. Probing Cell Surface Charge by Scanning Electrode Potential. *Electrophoresis* **2002**, *23*, 2080−2086.

(11) Ivošević DeNardis, N.; Ružić, I.; Pečar-Ilić, J.; El Shawish, S.; Ziherl, P. Reaction Kinetics and Mechanical Models of Liposome Adhesion at Charged Interface. *Bioelectrochemistry* **2012**, *88*, 48−56.

(12) Ivošević DeNardis, N.; Žutić, V.; Svetličić, V.; Frkanec, R. Adhesion Signals of Phospholipid Vesicles at an Electrified Interface. *J. Membr. Biol.* **2012**, *245*, 573−582.

(13) Ivošević DeNardis, N.; Pečar Ilić, J.; Ružić, I.; Pletikapić, G. Cell Adhesion and Spreading at a Charged Interface: Insight into the Mechanism using Surface Techniques and Mathematical Modelling. *Electrochim. Acta* **2015**, *176*, 743−754.

(14) Burgess, I.; Li, M.; Horswell, S. L.; Szymanski, G.; Lipkowski, J.; Majewski, J.; Satija, S. Electric Field-Driven Transformations of a Supported Model Biological Membrane—An Electrochemical and Neutron Reflectivity Study. *Biophys. J.* **2004**, *86*, 1763−1776.

(15) Xu, S. M.; Szymanski, G.; Lipkowski, J. Self-Assembly of Phospholipid Molecules at a Au(111) Electrode Surface. *J. Am. Chem. Soc.* **2004**, *126*, 12276−12277.

(16) Žutić, V.; Svetličić, V.; Zimmermann, A. H.; Ivošević DeNardis, N.; Frkanec, R. Comment on "Kinetics of the Adhesion of DMPC Liposomes on a Mercury Electrode. Effect of Lamellarity, Phase Composition, Size and Curvature of Liposomes, and Presence of the Pore Forming Peptide Mastoparan X. *Langmuir* **2007**, *23*, 8647−8649.

(17) Hellberg, D.; Scholz, F.; Schubert, F.; Lovrić, M.; Omanović, D.; Hernandez, V. A.; Thede, R. Kinetics of Liposome Adhesion on a Mercury Electrode. *J. Phys. Chem. B* **2005**, *109*, 14715−14726.

(18) Hernandez, V. A.; Scholz, F. The Lipid Composition Determines the Kinetics of Adhesion and Spreading of Liposomes on Mercury Electrodes. *Bioelectrochemistry* **2008**, *74*, 149−156.

(19) Tarek, M.; Tu, K.; Klein, M. L.; Tobias, D. J. Molecular Dynamics Simulations of Supported Phospholipid/Alkanethiol Bilayers on a Gold(111) Surface. *Biophys. J.* **1999**, *77*, 964−972.

(20) Vembanur, S.; Patel, A. J.; Sarupria, S.; Garde, S. On the Thermodynamics and Kinetics of Hydrophobic Interactions at Interfaces. *J. Phys. Chem. B* **2013**, *117*, 10261−10270.

(21) Acharya, H.; Vembanur, S.; Jamadagni, S. N.; Garde, S. Mapping Hydrophobicity at the Nanoscale: Applications to Heterogeneous Surfaces and Proteins. *Faraday Discuss.* **2010**, *146*, 353−365.

(22) Fortunelli, A.; Monti, S. Simulations of Lipid Adsorption on TiO2 Surfaces in Solution. *Langmuir* **2008**, *24*, 10145−10154.

(23) Schön, P.; Geerlings, J.; Tas, N.; Sarajlic, E. AFM Cantilever with in Situ Renewable Mercury Microelectrode. *Anal. Chem.* **2013**, *85*, 8937−8942.

(24) Hess, B.; Kutzner, C.; van der Spoel, D.; Lindahl, E. GROMACS 4: Algorithms for Highly Efficient, Load-Balanced, and Scalable Molecular Simulation. *J. Chem. Theory Comput.* **2008**, *4*, 435−447.

(25) Jorgensen, W. L.; Tirado-Rives, J. The OPLS [Optimized Potentials for Liquid Simulations] Potential Functions for Proteins,

939 Energy Minimizations for Crystals of Cyclic Peptides and Crambin. *J.*
940 *Am. Chem. Soc.* **1988**, *110*, 1657−1666.
941 (26) Berger, O.; Edholm, O.; Jahnig, F. Molecular Dynamics
942 Simulations of a Fluid Bilayer of Dipalmitoylphosphatidylcholine at
943 Full Hydration, Constant Pressure, and Constant Temperature.
944 *Biophys. J.* **1997**, *72*, 2002−2013.
945 (27) Jorgensen, W. L.; Chandrasekhar, J.; Madura, J. D.; Impey, R.
946 W.; Klein, M. L. Comparison of Simple Potential Functions for
947 Simulating Liquid Water. *J. Chem. Phys.* **1983**, *79*, 926−935.
948 (28) Hess, B.; Bekker, H.; Berendsen, H. J. C.; Fraaije, J. G. E. M.
949 LINCS: A Linear Constraint Solver for Molecular Simulations. *J.*
950 *Comput. Chem.* **1997**, *18*, 1463−1472.
951 (29) Miyamoto, S.; Kollman, P. A. Settle - an Analytical Version of
952 the Shake and Rattle Algorithm for Rigid Water Models. *J. Comput.*
953 *Chem.* **1992**, *13*, 952−962.
954 (30) Christen, M.; Hünenberger, P. H.; Bakowies, D.; Baron, R.;
955 Bürgi, R.; Geerke, D. P.; Heinz, T. N.; Kastenholz, M. A.; Kräutler, V.;
956 Oostenbrink, C. The GROMOS Software for Biomolecular Simu-
957 lation: GROMOS05. *J. Comput. Chem.* **2005**, *26*, 1719−1751.
958 (31) Vernier, P. T.; Li, A. M.; Marcu, L.; Craft, C. M.; Gundersen, M.
959 A. Ultrashort Pulsed Electric Fields Induce Membrane Phospholipid
960 Translocation and Caspase Activation: Differential Sensitivies of
961 Jurkat T Lymphoblasts and Rat Glioma C6 cells. *IEEE Trans. Dielectr.*
962 *Electr. Insul.* **2003**, *10*, 795−809.
963 (32) Humphrey, W.; Dalke, A.; Schulten, K. VMD: Visual Molecular
964 Dynamics. *J. Mol. Graphics* **1996**, *14*, 33−38.
965 (33) Moscho, A.; Orwar, O.; Chiu, D. T.; Modi, B. P.; Zare, R. N.
966 Rapid Preparation of Giant Unilamellar Vesicles. *Proc. Natl. Acad. Sci.*
967 *U. S. A.* **1996**, *93*, 11443−11447.
968 (34) Žutić, V.; Kovač, S.; Tomaić, J.; Svetličić, V. Heterocoalescence
969 between Dispersed Organic Microdroplets and a Charged Conductive
970 Interface. *J. Electroanal. Chem.* **1993**, *349*, 173−186.
971 (35) Ivoševic, N.; Žutić, V. Spreading and Detachment of Organic
972 Droplets at an Electrified Interface. *Langmuir* **1998**, *14*, 231−234.
973 (36) Ivošević, N.; Žutić, V.; Tomaić, J. Wetting Equilibria of
974 Hydrocarbon Droplets at an Electrified Interface. *Langmuir* **1999**, *15*,
975 7063−7068.
976 (37) Israelachvili, J. N. *Intermolecular and Surface Forces*, Revised 3rd
977 ed.; Academic Press: New York, 2011.
978 (38) Tsekov, R.; Kovač, S.; Žutić, V. Attachment of Oil Droplets and
979 Cells on Dropping Mercury Electrode. *Langmuir* **1999**, *15*, 5649−
980 5653.
981 (39) Zawisza, I.; Bin, X.; Lipkowski, J. Potential-Driven Structural
982 Changes in Langmuir-Blodgett DMPC Bilayers Determined by in situ
983 Spectroelectrochemical PM IRRAS. *Langmuir* **2007**, *23*, 5180−5194.
984 (40) Moncelli, M. R.; Becucci, L.; Guidelli, R. The Intrinsic pKa
985 Values for Phosphatidylcholine, Phosphatidylethanolamine, and
986 Phosphatidylserine in Monolayers Deposited on Mercury Electrodes.
987 *Biophys. J.* **1994**, *66*, 1969−1980.
988 (41) Scatena, L.; Brown, M.; Richmond, G. Water at Hydrophobic
989 Surfaces: Weak Hydrogen Bonding and Strong Orientation Effects.
990 *Science* **2001**, *292* (5518), 908−912.
991 (42) Shen, Y. R.; Ostroverkhov, V. Sum-Frequency Vibrational
992 Spectroscopy on Water Interfaces: Polar Orientation of Water
993 Molecules at Interfaces. *Chem. Rev.* **2006**, *106* (4), 1140−1154.
994 (43) Vácha, R.; Rick, S. W.; Jungwirth, P.; de Beer, A. G.; de Aguiar,
995 H. B.; Samson, J.-S.; Roke, S. The Orientation and Charge of Water at
996 the Hydrophobic Oil Droplet−Water Interface. *J. Am. Chem. Soc.*
997 **2011**, *133* (26), 10204−10210.
998 (44) Stoodley, R.; Bizzotto, D. Epi-Fluorescence Microscopic
999 Characterization of Potential-Induced Changes in a DOPC Monolayer
1000 on a Hg Drop. *Analyst* **2003**, *128*, 552−561.
1001 (45) Ziegler, M. J.; Vernier, P. T. Interface Water Dynamics and
1002 Porating Electric Fields for Phospholipid Bilayers. *J. Phys. Chem. B*
1003 **2008**, *112*, 13588−13596.
1004 (46) Van der Spoel, D.; Lindahl, E.; Hess, B.; Groenhof, G.; Mark, A.
1005 E.; Berendsen, H. J. C. GROMACS: Fast, Flexible, and Free. *J.*
1006 *Comput. Chem.* **2005**, *26*, 1701−1718.

1007 (47) Levine, Z. A.; Vernier, P. T. Life Cycle of an Electropore: Field-
1008 Dependent and Field-Independent Steps in Pore Creation and
1009 Annihilation. *J. Membr. Biol.* **2010**, *236*, 27−36.
1010 (48) Marino, K. A.; Bolhuis, P. G. Confinement-Induced States in the
1011 Folding Landscape of the Trp-cage Miniprotein. *J. Phys. Chem. B* **2012**,
1012 *116*, 11872−11880.
1013 (49) Sugita, Y.; Okamoto, Y. Replica-Exchange Molecular Dynamics
1014 Method for Protein Folding. *Chem. Phys. Lett.* **1999**, *314*, 141−151.
1015 (50) Yu, J.; Kan, Y.; Rapp, M.; Danner, E.; Wei, W.; Das, S.; Miller,
1016 D. R.; Chen, Y.; Waite, J. H.; Israelachvili, J. N. Adaptive Hydrophobic
1017 and Hydrophilic Interactions of Mussel Foot Proteins with Organic
1018 Thin Films. *Proc. Natl. Acad. Sci. U. S. A.* **2013**, *110*, 15680−15685.
1019 (51) Kotyńska, J.; Figaszewski, Z. Adsorption Equilibria between
1020 Liposome Membrane Formed of Phosphatidylcholine and Aqueous
1021 Sodium Chloride Solution as a Function of pH. *Biochim. Biophys. Acta,*
1022 *Biomembr.* **2005**, *1720*, 22−27.
1023 (52) Burgess, I.; Zamlynny, V.; Szymanski, G.; Lipkowski, J.;
1024 Majewski, J.; Smith, G.; Satija, S.; Ivkov, R. Electrochemical and
1025 Neutron Reflectivity Characterization of Dodecyl Sulfate Adsorption
1026 and Aggregation at the Gold-Water Interface. *Langmuir* **2001**, *17*,
1027 3355−3367.